Macroscopic strength and Failure properties of Flow-Drill Screw Connections

Johan Kolstø Sønstabø[*, a], Petter Henrik Holmstrøm[a, b], David Morin[a, b], Magnus Langseth[a, b]

*Corresponding author. Tel.: +47 476 31 726. E-mail address: johan.k.sonstabo@ntnu.no.
[a]Department of Structural Engineering, Norwegian University of Science and Technology, Rich. Birkelandsvei 1a, N-7491 Trondheim, Norway
[b]Structural Impact Laboratory (SIMLab), Centre for Research-based Innovation, Norwegian University of Science and Technology, Rich. Birkelandsvei 1a, N-7491 Trondheim, Norway.

Abstract

Force-displacement responses and failure behaviour of connections using flow-drill screws to join aluminium sheets were investigated under various quasi-static loading conditions. This included single connector tests under tensile, shear and combined tensile and shear loadings, using cross test coupons in a new test set-up, and peeling and single lap-joint tests. The strength of the connection increased with the amount of shear loading, while the ductility decreased. No effect of the anisotropy of the sheets on the behaviour in the single connector tests was found. Axial crushing tests of aluminium single-hat sections joined with flow-drill screws were also performed. Two connection failure modes not observed during the single connector test were found in these tests. For comparison, equivalent single connector and component tests were carried out for self-piercing rivet connections. Similar trends with respect to the ductility, maximum force and shape of force-displacement curves were observed for the two connections, but the local failure modes were different.

Keywords: Flow-Drill Screw, Self-Piercing Rivet, Connection, Aluminium, Quasi-static, Dynamic

Introduction

Joining with Flow-Drill Screws (FDS) is a technology which may be used to join a variety of dissimilar materials, and is increasingly used to join aluminium parts in the load bearing structure of cars. By this technique sheets, extrusions, castings or combinations of these may be joined with a high strength steel screw. The joining process is a one-step procedure consisting of six stages, as shown in Fig. 1: (a) warming up due to friction between the screw and the sheet, (b) penetration of the sheet material, (c) forming of the draught, (d) thread forming, (e) full thread engagement and (f) tightening (EJOT). A pilot hole is usually drilled in the top sheet prior to joining. One of the main advantages with this technology is that tool access only is required from one side of the assembly. This may enable the process to be used in configurations where other joining techniques fail.

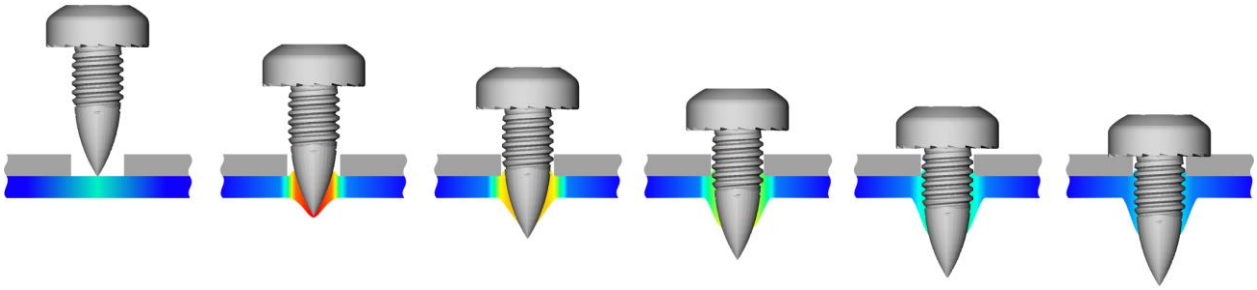

Fig. 1: Different stages of the flow-drill screw process. a): warming up. b): penetration of the material. c): forming of the draught. d): thread forming. e): full thread engagement. f): tightening.

The FDS process is based on the technology of flow drilling (also called form drilling, thermal drilling or friction drilling), which is a method for making holes in metals; see e.g. Head et al. (1984). A synthesis of several studies on the flow-drilling process was given by Miller and Shih (2006), including measurement of thrust force and torque, study of microstructural alterations, flow drilling of cast metals, tool wear and analytical and finite element modelling. A literature survey revealed no publications concerning the FDS process.

No publications have been found on connecting two aluminium sheets with flow-drill screws. However, an experimental study of FDS connections was published by Szlosarek et al. (2013), who investigated the behaviour of a carbon-fibre-reinforced polymer plate joined to an aluminium plate. They performed tests by loading the connection in shear, tension and different combinations of shear and tension, and found that the failure load was similar for all load combinations, but observed two different failure modes.

Even though little information about FDS connections is found in the open literature, other related joining technologies used in the automotive industry, e.g. resistance spot welding and self-piercing riveting, have been widely covered and can be used as guidelines for experimental studies of FDS connections. Examples of experimental strategies for characterization of connections are presented in the following.

The common approach to study the behaviour of connections is to subject test coupons, consisting of a single connector joining two metal plates, to different controlled macroscopic load paths. Typical paths are tensile, shear, different combinations of tensile and shear and peeling loads.

Pedreschi and Shinha (1996) investigated the potential of press-joining in cold-formed steel structures by means of a series of lap-shear and bending tests. Lennon et al. (1999) did a comparative investigation of the mechanical behaviour of clinching, self-piercing rivet, pop rivet and self-tapping screw connections in thin gauge steel using the shear dominated lap-joint test. Similarly, Di Lorenzo and Landolfo (2004) carried out a comparative study of the shear response of blind rivets, circular press-joints and self-piercing rivets joining two and three steel sheets. The lap-joint specimen was used in the tests, with two connections in each sample. Briskham et al. (2006) performed lap-shear and peeling tests to assess the functional suitability of self-piercing rivet, resistance spot weld and spot friction joint connections for use in aluminium automotive structures.

Langrand et al. (2002) carried out experimental studies on the behaviour of blind rivets, which are commonly used in modern fighters and commercial aircraft frameworks. They did quasi-static and dynamic single connector tests on aluminium tension and lap-joint specimens instrumented with strain gauges.

The spot welded connection is probably the most investigated connection type used in the automotive industry. Lee et al. (1998) utilized a special designed test fixture similar to the Arcan type set-up (Arcan et al., 1987) to investigate the quasi-static behaviour of spot welded steel coupons under tensile, shear and various combined loadings. Wung (2001) carried out lap-shear, in-plane rotation, peeling, normal separation as well as different combined loading mode tests. In addition, a more sophisticated test with a more complex combined load path was performed (Wung et al., 2001). Langrand and Combescure (2004) used an Arcan type test to characterize the spot weld behaviour under tensile, shear and combined loading modes, and performed tensile pull-out, single lap-shear and peeling tests. This work was extended by Langrand and Markiewicz (2010) to include dynamic testing.

Self-piercing riveting (SPR) is a joining technology similar to FDS. The shear, tensile and combined shear and tensile quasi-static load responses of SPR connections between aluminium extrusions were investigated by Porcaro et al (2006a). They also studied the influence of the plate thickness, rivet geometry, material properties and loading conditions (Porcaro et al., 2006b), and conducted dynamic tests to assess the rate effect on the behaviour of SPR connections (Porcaro et al., 2008). Sun and Khaleel (2005) investigated the quasi-static behaviour of SPR connections using

cross-shaped tension specimens. This work was extended to also include dynamic testing (Sun and Khaleel, 2007). Similar and dissimilar materials were joined, and tests were carried out using cross tension, lap-shear and peeling specimens.

As there is a lack of knowledge about the behaviour of FDS connections in the peer-review literature, thorough experimental studies are required on this topic to provide a better understanding of the connections in order to allow for reliable designs of future vehicle structures.

Based on previous work on mechanical fasteners an experimental programme was carried out to investigate the behaviour of single connector FDS connections under various quasi-static loading conditions. In addition, quasi-static and dynamic component tests were carried out in order to investigate the structural behaviour of the connections under complex, non-controlled load paths. To assess the behaviour of FDS connections compared to other mechanical fasteners, an equivalent experimental programme was carried out for SPR connections.

Connector and sheet material

In this work it is distinguished between the terms "connector" and "connection". The term "connection" is here defined as *the system which mechanically fastens two or more parts together*. This definition is based on the definition of a connection in Eurocode 9 (CEN, 2007). The "connector" is in this work *the steel screw that is used to form the connection*. Thus, the connection is the system comprised of the connector and the surrounding aluminium sheet material (see Fig. 2 a)).

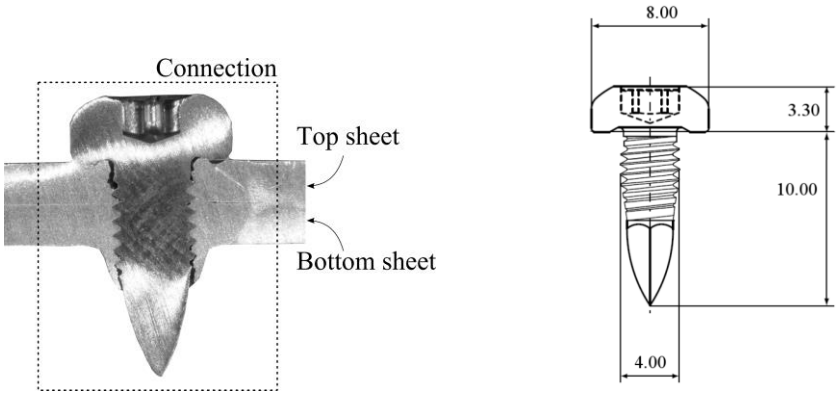

a) Cross-section of connection. b) Geometry of connector.

Fig. 2: Connection and connector.

The connector used herein was an M4 screw with a nominal length of 10 mm, made of case hardened mild steel, with standard tip and produced by EJOT. A cross-sectional view of the connection and the geometry of the connector are shown in Fig. 2 a) and b), respectively.

The plates used in the single connector and component tests were rolled sheets of AA 6016 in temper T4 with a nominal thickness of 2 mm. Due to the rolling procedure such sheets usually exhibit orthotropic plastic anisotropy (Lademo et al., 2009).

In order to assess the strength and anisotropy of the sheet material, uniaxial tensile tests were carried out in seven different directions with respect to the rolling direction. Fig. 3 shows the results in terms of (a) engineering stress and strain curves to the onset of diffuse necking and (b) plastic strain ratios. The plastic strain ratio in the direction α with respect to the rolling direction is defined as $R_\alpha = \dot{\epsilon}^p_w / \dot{\epsilon}^p_t\big|_\alpha$, where $\dot{\epsilon}^p_w$ and $\dot{\epsilon}^p_t$ are the true plastic strain increments in the width and thickness directions, respectively. It is seen from Fig. 3 a) that the sheets exhibited significant ductility and work hardening, but no significant anisotropy with respect to the strength. From Fig. 3 b) it is evident that they exhibited significant plastic anisotropy.

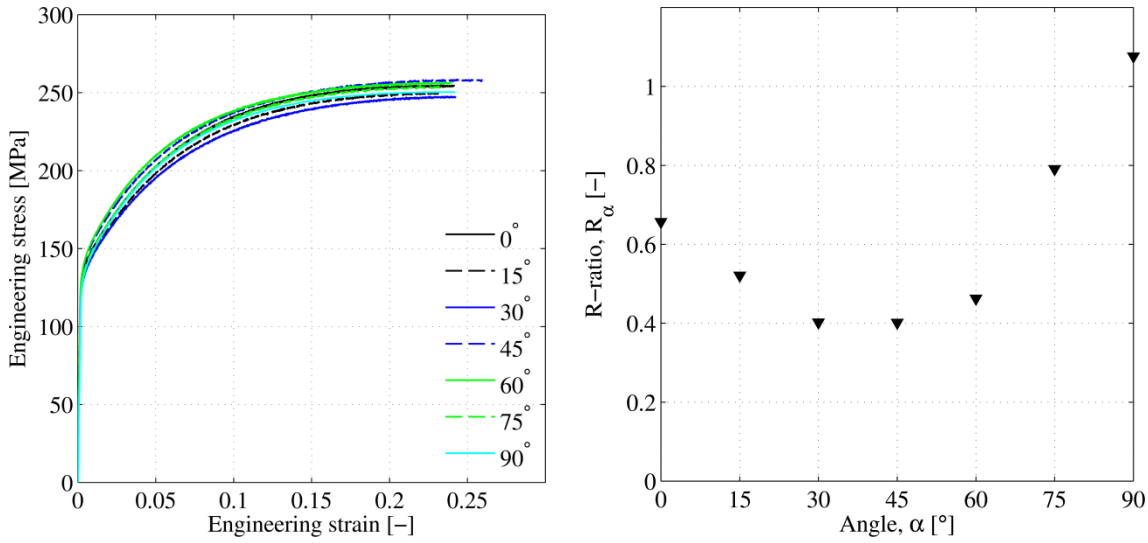

a) Engineering stress and strain curves.

b) Plastic strain ratios.

Fig. 3: Results from uniaxial tensile tests in seven different directions with respect to the rolling direction of the sheets.

Experimental programme and test set-up

An extensive experimental programme consisting of two parts was defined (Table 1); one part with single connector tests and one with component tests. In the first part, different quasi-static loading conditions were investigated using cross, single lap-joint and peeling specimens with a single connector. In the cross tests the connection was tested for three different loadings: tensile, combined tensile and shear and shear loading. Based on the work of Porcaro et al. (2008) on SPR connections, it was assumed that there were no significant rate effects on the behaviour of the single FDS connections. Thus, the single connector tests were limited to quasi-static tests.

The second part of the test programme consisted of quasi-static and dynamic axial crushing of single-hat sections. Due to the progressive buckling occurring in such tests the connections are subjected to complex and non-controlled load paths. Furthermore, as the folding – and thus the behaviour of the connections – depends on the impact velocity, this component test provides conditions similar to a real case scenario. Emphasis was put on the dynamic component tests, while the quasi-static tests served as reference to estimate the dynamic effects on energy absorption of the components and failure modes of the connections.

In the following, the experimental test set-up is explained, first for each single connector test and subsequently for the component tests.

Table 1
Test matrix for experimental programme.

	Test type	Orientation of sheet rolling direction		Loading angle θ	Repetitions
		Top sheet	Bottom sheet		
Single connector tests	Cross (tensile)	Transversal	Longitudinal	90	4
	Cross (mixed)	Transversal	Longitudinal	45	3
	Cross (shear)	Transversal	Longitudinal	0	5
	Single lap-joint	Longitudinal	Longitudinal		4
	Single lap-joint	Transversal	Transversal		3
	Peeling	Transversal	Transversal		3
Component tests	Quasi-static crushing	Longitudinal	Longitudinal		2
	Dynamic crushing	Longitudinal	Longitudinal		3

Single connector tests

It is important to understand that the loading conditions discussed herein, i.e. “tensile loading”, “mixed tensile and shear loading” and “shear loading”, are from a global, macroscopic perspective.

The local loading conditions within the connection and on the connector itself are complex and unknown and changes continuously throughout the tests. For instance, in the cross shear tests - which arguably may be considered as “pure shear” from a macroscopic perspective - the screw is loaded in shear in the start, but after a while the connection deforms and the screw starts to rotate, introducing a more complex loading situation within the connection.

The geometry of the cross specimens is shown in Fig. 4 a). The specimens consisted of two rectangular sheets connected with a single connector in the centre. A specially designed testing rig based on the set-up of Porcaro et al. (2004) was adapted (illustrated in Fig. 4 b) and c)). With this testing rig the combination of macroscopic tensile and shear loads was controlled. The ratio of macroscopic tensile and shear load was exactly defined by the loading angle θ; see Fig. 4 b). The load application line was defined by two pull-bars, and the test set-up was designed such that this line intersected the specimen plane at the centre of the connection (see Fig. 4 a)). The pull-bars were clamped to the crosshead of the testing machine. In this work, three different loading angles were considered: 90º, 45º and 0º. The holes in the cross specimens (see Fig. 4 a)) were used for clamping the specimen to the testing rig using massive steel blocks and bolts. The rolling directions of the sheets are indicated with arrows in Fig. 4 a). The shear loads were applied normal to the rolling direction.

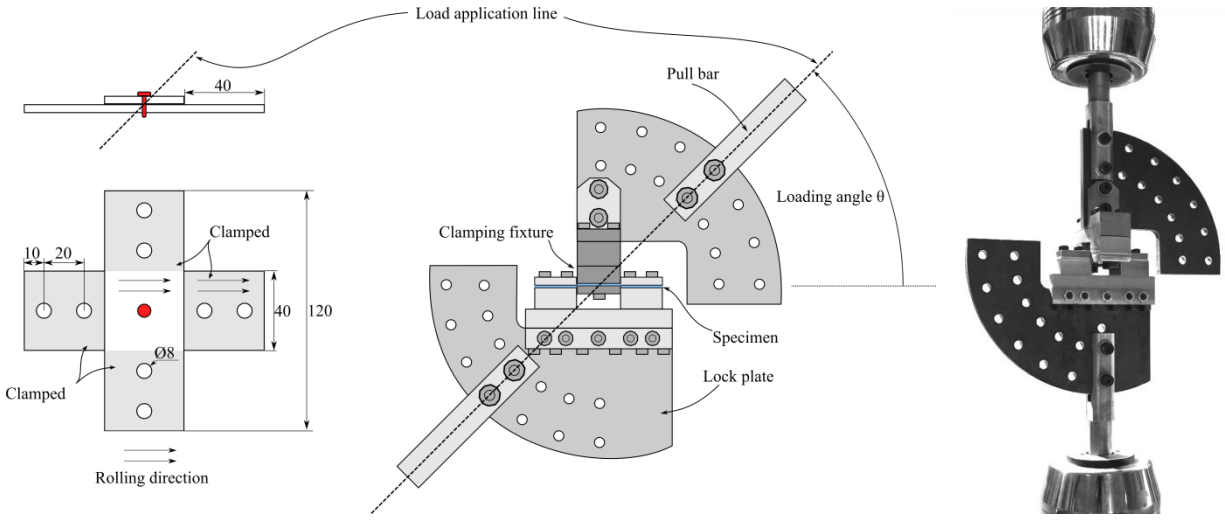

a) Geometry of specimen. b) Schematic illustration of testing rig c) Picture of testing rig

Fig. 4: Cross test set-up.

The single lap-joint specimen is shown in Fig. 5 a) and b). It consisted of two rectangular plates joined with a single connector in the centre of an overlap area. To evaluate the effect of sheet anisotropy on the behaviour of the connection, single lap-joint tests were carried out on specimens with the sheet rolling direction oriented in both the longitudinal (Fig. 5 a)) and transversal (Fig. 5 b)) direction of the specimen. The peeling specimen (Fig. 5c)) consisted of two identical bent plates joined with a single connector at the short flange. Each end of the single lap-joint and peeling specimen was clamped using mechanical grips. The grips were aligned along the load application line of the test machine without any offset. Hence, the single lap-joint specimens were slightly deformed when tightening the grips. The deformation was purely elastic, and is shown schematically in Fig. 5 d).

All single connector tests were carried out under displacement control at a displacement velocity of 10 mm/min. Force and displacement histories were recorded. Additionally, the single lap-joint and peeling specimens were instrumented with an extensometer (50 mm gauge length). The tests were terminated when the force level reached zero.

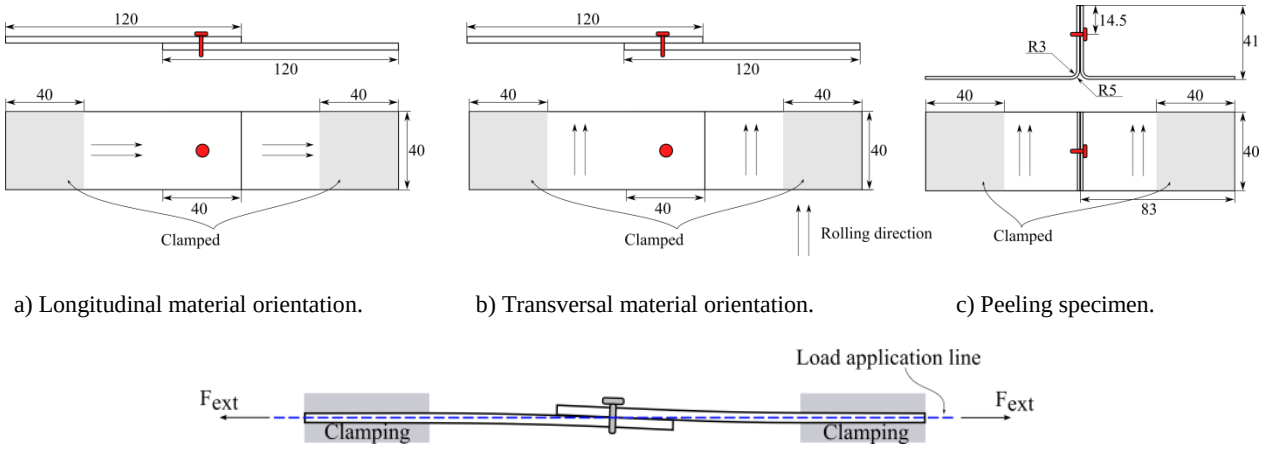

a) Longitudinal material orientation. b) Transversal material orientation. c) Peeling specimen.

d) Clamping deformation in single lap-joint test.

Fig. 5: Single lap-joint and peeling test set-up.

Component tests

Fig. 6 shows the geometry of the single-hat specimen, which consisted of a flat and a hat-shaped sheet. The hat shape was obtained by four bending operations, and connected to the flat sheet with

ten equally spaced screws on each flange. The rolling direction of the sheets was oriented in the longitudinal direction of the component.

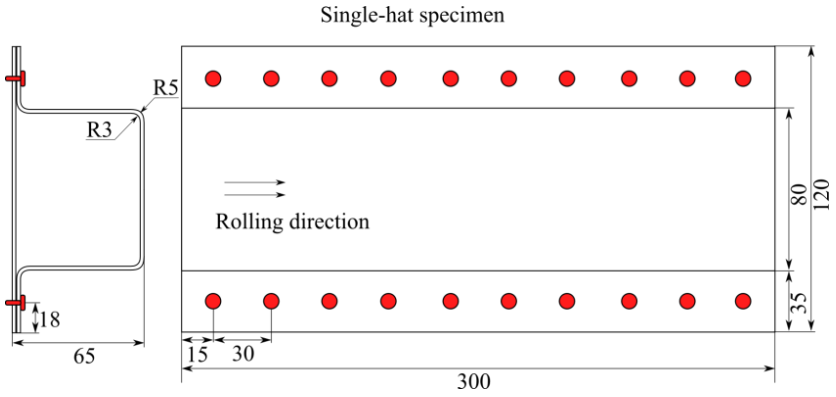

Fig. 6: Geometry of single-hat specimen.

A pendulum accelerator was employed to conduct the dynamic axial crushing tests. Cf. Hanssen et al. (2003) for a detailed description of the test set-up. The impacting mass was 395.5 kg and the velocity was approximately 10 m/s.

The specimen was positioned in the test machines such that the centre line of the impactor was aligned with the centre line of the specimen, using a custom made clamping fixture (Fig. 7).

In order to ensure the same progressive buckling mode in all crushing tests and to minimize the scatter in the results, the specimens were manually triggered prior to the tests with a geometrical imperfection at the end facing the impactor (see Fig. 7 c)).

The quasi-static component tests were carried out under displacement control with a velocity of 10 mm/min, using the same clamping device as for the dynamic tests. Total crushing distance was 150 mm.

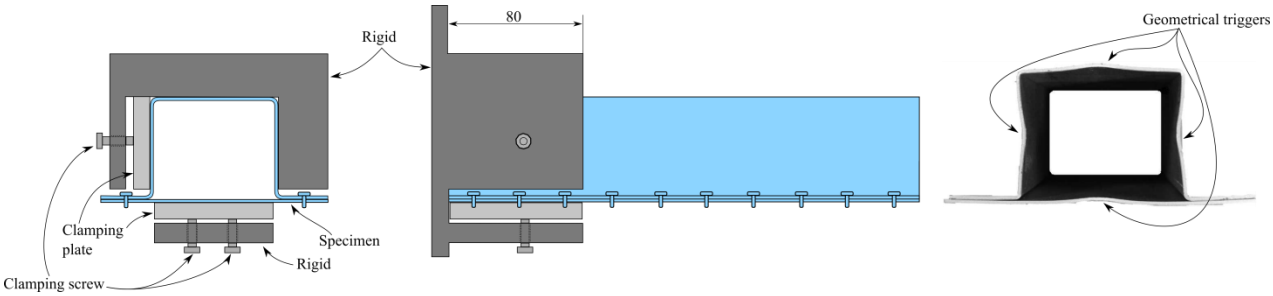

a) Top view. b) Side view. c) Triggers.

Fig. 7: Schematic illustration of clamping device used in crushing tests. Geometrical triggers are indicated in c).

Experimental results

In this section the results from the FDS single connector and component tests are presented and discussed.

Single connector tests

The force-displacement curves from the cross tests are shown in Fig. 8. The tensile mode exhibits lowest force and highest ductility, while the shear mode exhibits highest force and lowest ductility. The mixed mode results show intermediate force level and ductility. The repeatability of the test results was acceptable.

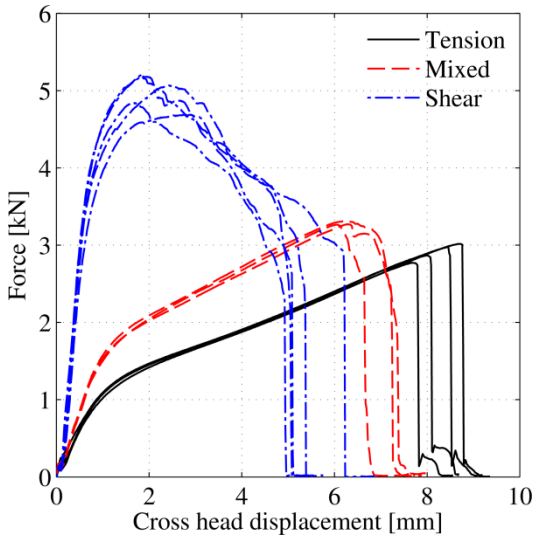

Fig. 8: Force-displacement curves from cross tests.

No visible plastic deformations were observed in the screws (which was the case for all single connector tests). Details of the separated cross specimens are shown in Fig. 9.

Under pure tensile loading the sheets deformed until a critical force was reached. The knee in the force-displacement curves corresponds to yielding of the sheets. A rapid failure occurred quickly after the force peak. By inspecting Fig. 9 a) and d) it is evident that the connection failed due to thread stripping of the bottom sheet material. As seen, some residue material was visible on the screw after failure, indicating that the threads in the bottom sheets were broken off due to shear fracture.

A similar force-displacement relationship was observed in the tests with combined tensile and shear loadings. Yielding of the sheet material caused also for these tests a knee in the force-displacement curve, and after the maximum force was reached, softening occurred before a rapid failure terminated the test. During deformation a slight rotation of the screw was observed, resulting in thread engagement mostly on one side of the screw hole. Thread stripping therefore occurred on this side of the screw hole, again of the bottom sheet. This is clearly seen in Fig. 9 b) and e). On one side the threads remained relatively intact; on the other side they were stripped.

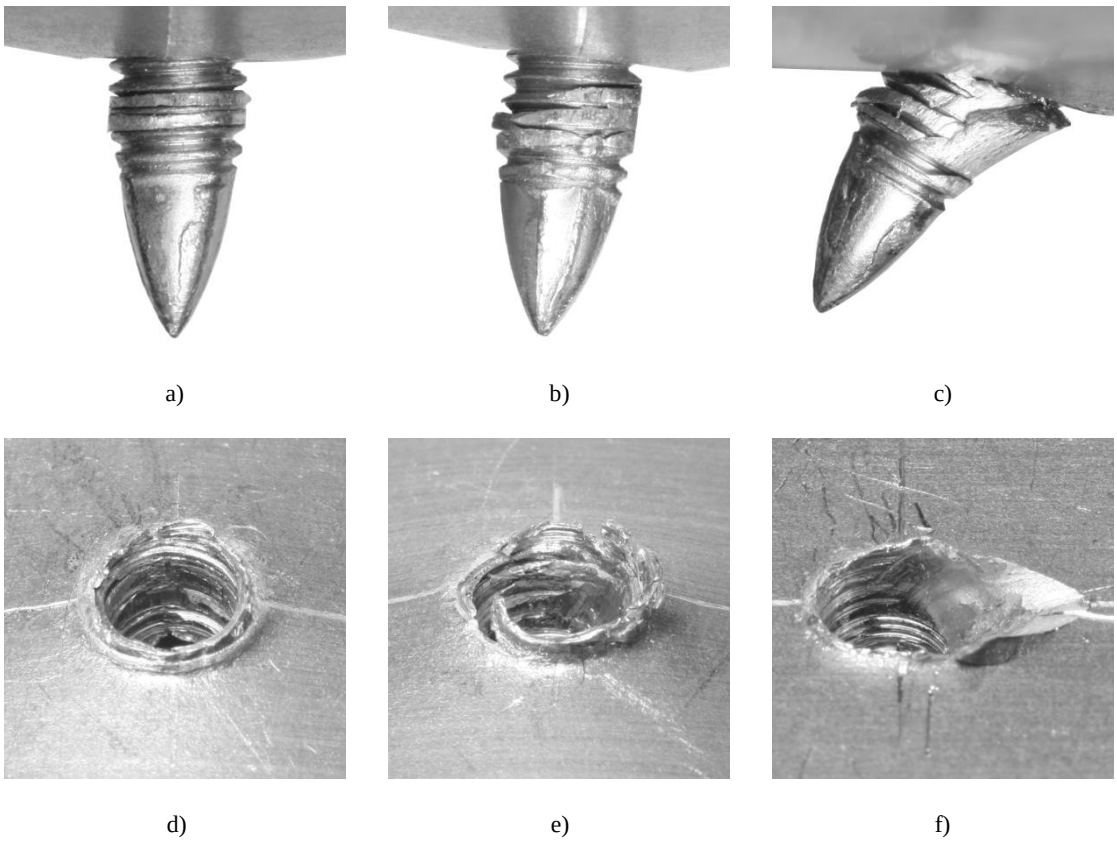

Fig. 9: Details of separated cross specimens. a), b) and c): residue material on screws after separation for tensile, mixed and shear loading cases, respectively. d), e) and f): screw hole in bottom sheet (viewed from the top side) after separation for tensile, mixed and shear loading cases, respectively.

Under pure shear loading a stiffer response was observed until maximum force was reached. As the connection was further loaded, the screw gradually rotated up to 30-40 degrees. During this rotation the threads on one side of the screw hole were gradually disengaged in a similar manner as observed for the combined loading case, leading to a gradual decrease of force to about 60 percent of maximum force after the peak (see Fig. 8). The rotation and thread disengagement on one side led to failure of the bottom sheet material at the loaded side of the screw hole, such that the screw

was pulled out. This corresponds to the abrupt decrease of force at the end of the test. The failure differed from what was found for tensile and mixed loadings. As seen in Fig. 9 c) and f), a more significant amount of residue material remained attached to the screw after failure, indicating that failure occurred by through thickness shear fracture of the bottom sheet material, rather than thread stripping.

A similar force response as in the cross shear tests was observed for the single lap-joint tests, see Fig. 10. This was expected, since the loading conditions on the connection in the two tests were similar. After approximately 80 percent of maximum force was reached, the force level flattened out and increased slowly until maximum force. After maximum force was reached the force decreased almost linearly to approximately 60 percent of maximum force, where the connection failed.

From Fig. 10 it is evident that the effect of the sheet anisotropy on the force-displacement response is negligible from a design point of view. Furthermore, no effect of the sheet anisotropy was observed on the deformation and failure of the connection.

The specimen deformation is shown in Fig. 11. Also here rotation of the screw due to the shear force led to a one-sided thread engagement and a through thickness shear fracture of the bottom sheet material, see Fig. 11 b) and c). The screw rotation caused bending deformations of the top sheet near the screw, as seen in Fig. 11 a). This was not observed in the shear cross tests, due to the more restrictive clamping in the cross tests.

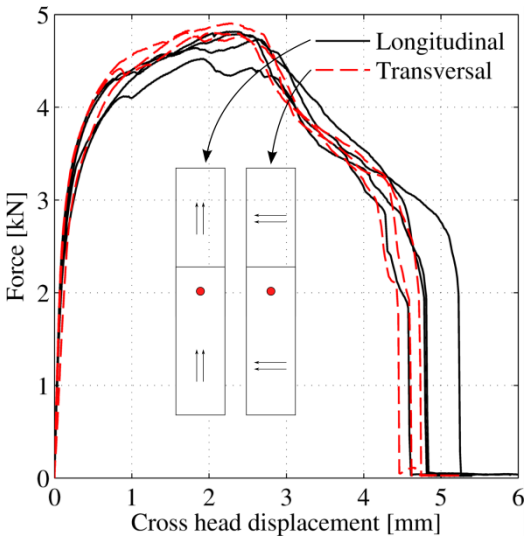

Fig. 10: Force-displacement curves from single lap-joint tests. Results from both material orientations are shown.

a) Specimen.

b) Top side of bottom sheet.

c) Underside of top sheet.

Fig. 11: Deformed single lap-joint specimen.

The force-displacement curves from the peeling tests are given in Fig. 12. The force increased rapidly at first, until the sheets yielded. A rapid fracture occurred immediately after maximum force was reached.

A representative deformed peeling specimen is shown in Fig. 13. As the load increased, the bends in the L-shaped plates were stretched out, resulting in new bends in the sheets around the screw. The screw head stiffened the top sheet, resulting in rotation of the screw and asymmetry in the bending deformations, as may be seen in Fig. 13 a) (the bottom sheet is bent more). Failure occurred by stripped threads in the bottom sheet, as may be seen in Fig. 13 b) and c), where the screw and screw hole are depicted after failure.

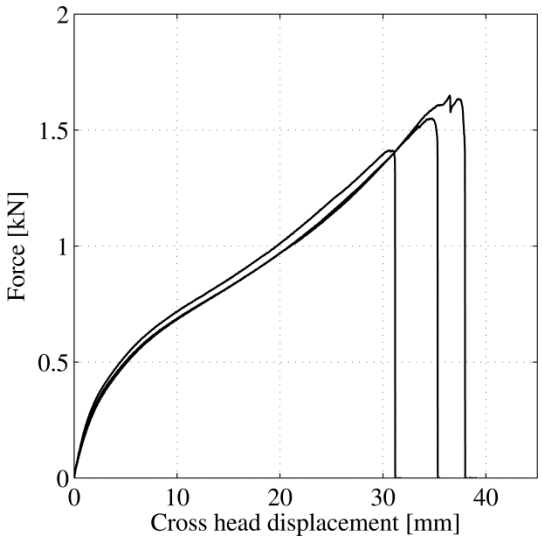

Fig. 12: Force-displacement curves from peeling tests.

a) Specimen.

b) Top side of bottom sheet.

c) Screw.

Fig. 13: Deformed peeling specimen.

The load on the connection in the peeling tests was tensile dominated. However, compared to the cross tension tests it is evident that the global strength of the connection was reduced under peeling loading. This may partially be explained by the presence of a lever force. Fig. 14 illustrates the forces acting on one part of the specimen in the start of the test, where the lever force is idealized as a concentrated force for simplicity. By force equilibrium it is obvious that the force transferred

through the screw connection in this test is higher than the external force. Thus, as expected the connection failed for a smaller external load than under pure tensile loading.

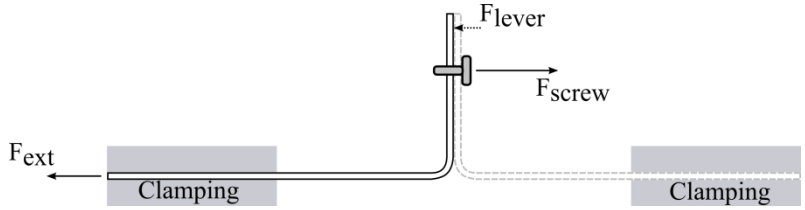

Fig. 14: Illustration of lever effect in peeling test.

Component tests

The force-displacement and mean force-displacement histories for the component tests are shown in Fig. 15 a) and b), respectively. Little scatter was observed. The mean force was approximately 15-20 % higher for the dynamic compared to the quasi-static tests. Since strain rate effects are small for this material (Moore and Bate, 2002), the main reason for the increased energy absorption in the dynamic test is lateral inertia forces set up in the profile during progressive folding.

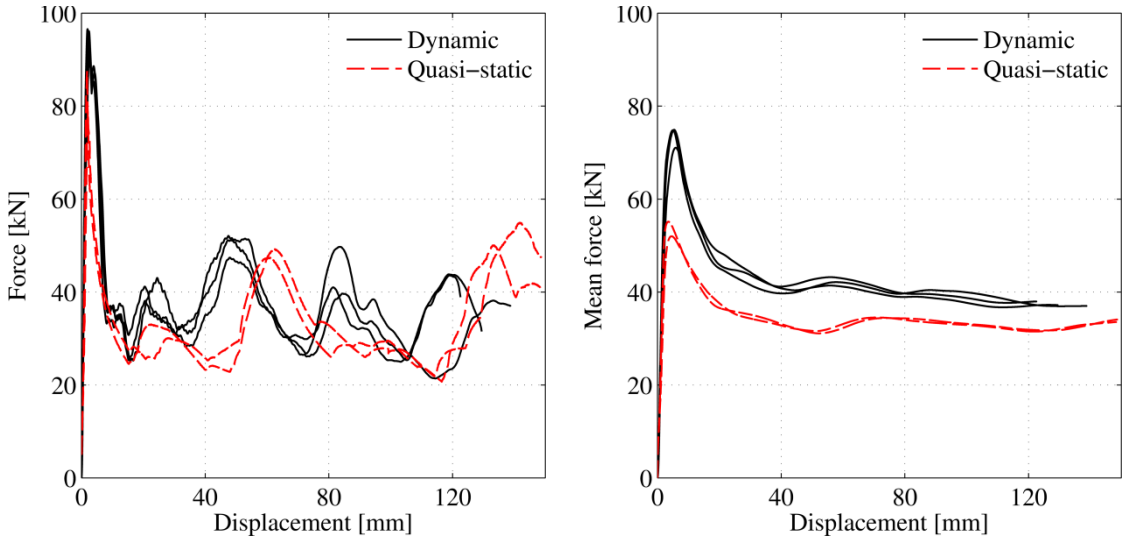

a) Force-displacement curves.

b) Mean force-displacement curves.

Fig. 15: Force-displacement (a) and mean force-displacement (b) curves from dynamic and quasi-static axial crushing tests.

A deformed sample from the dynamic test is pictured in Fig. 16. After the tests, four lobes were clearly visible in each specimen. The creation of a fifth lobe was interrupted by the clamping and the termination of the tests. The same progressive buckling mode was observed in the dynamic and

quasi-static tests; only minor differences were observed in the pattern. Differences in the force-displacement responses between quasi-static and dynamic tests may be explained by the differences in initial geometrical imperfections and thus the buckling pattern.

Some cracks were observed in the sheets, located in tensile dominated zones in the lobes at the corner of the specimens, where large plastic strains occurred both during forming of the single-hat and during crushing. The global response is not believed to be affected by the crack formations.

Fig. 16: Deformed single-hat section from dynamic axial crushing test, viewed from different directions.

The deformation of each screw connection was investigated closely after the tests, and four deformation and fracture modes were found: screw rotation, screw pull-out, screw push-out and shear fracture of screws, depicted in Fig. 17 a). The figure includes a graphical illustration where lines indicate for which screws the different modes were observed in the dynamic tests. The screw positions are numbered from 1 to 7, and the corresponding positions are shown for a representative deformed specimen in Fig. 17 b). The same modes were observed in the quasi-static tests, except for the shear fracture.

Deformation took place in the sheet material. Other than the shear fracture observed in the dynamic tests, no visible deformation occurred to any of the screws.

Rotation of screws was caused by relative movement between the sheets, and was the most frequent mode; over half of the screws experienced this mode. It was observed in all screw positions except for position 4. This mode is closely related to the deformation observed in the cross shear and single lap-joint tests.

The screw pull-out mode is related to the deformation observed in the cross tension tests. It was observed for screws in positions 1, 5 and 6, and was often seen together with screw rotation.

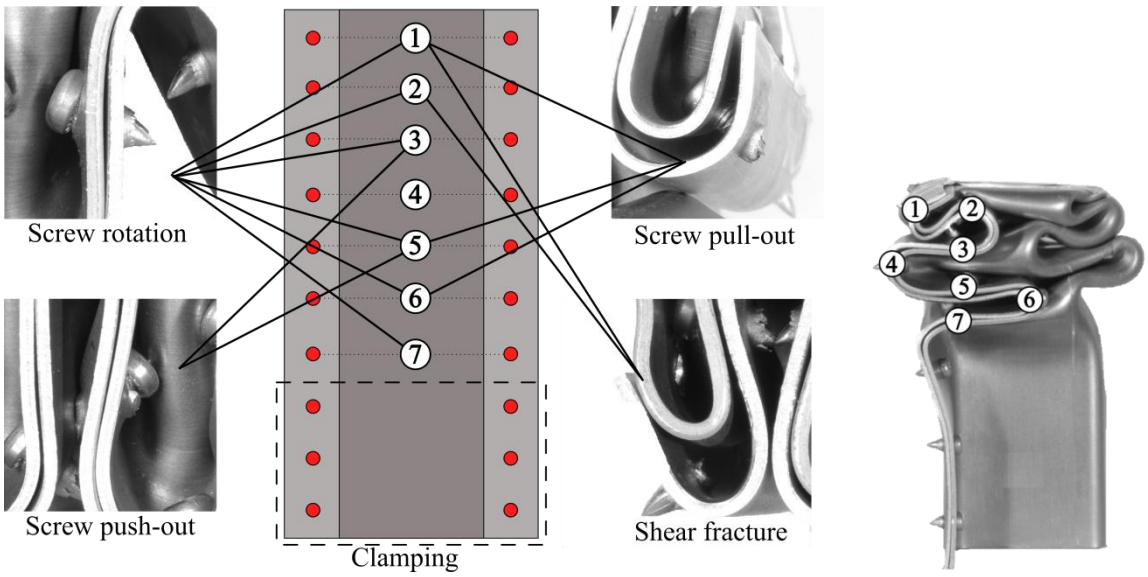

a) Pictures and locations of screw deformation and fracture modes. b) Screw positions after crushing.

Fig. 17: Graphical illustration of the observations of screw deformation and failure modes in the dynamic tests. Screw positions are indicated with numbers, both positions on the deformed specimens (a) and initial positions (b). The different lines (b) indicate where the screw deformation modes were observed.

Screw push-out occurred when the tail of the screw had contact with other parts of the specimen during buckling, and was observed in straight parts between lobes (position 3 and 5). The push-out mode was not observed in the single connector tests.

Two screws fractured near the screw head in the dynamic tests. These screws were located near the impacted end of the specimen (positions 1 and 2). The reason for this fracture mode is not well understood, but could be a result of over-torqueing during the screwing process, dynamic effects in the tests, or both.

As seen in Fig. 17, no connections in position 4 had visible deformation in the dynamic tests. These screws were located at the middle of the second outward lobe where little relative movement between the sheets occurred.

While both the screw rotation and pull-out modes also were observed in the single connector tests, the push-out and shear fracture modes only occurred in the component tests. This could be important from a finite element modelling perspective. In large-scale shell simulations (for instance full-scale car crash simulations) connections are typically represented by simple constraint-based

macroscopic models representing the physical behaviour of the connections. Such models are usually calibrated using single connector tests (e.g. cross tests) and validated with component tests. Thus, physical behaviour only observed in the component tests (such as the push-out and shear fracture modes in this case) will not be represented by the macroscopic models.

Comparison with self-piercing rivet connections

The rivets used were of the Böllhof standard, type C-SKR, made of high strength steel with a nominal diameter of 5 mm, which is a typical rivet used in the automotive industry. The geometry of the rivet and the cross-section of the rivet connection are shown in Fig. 18. A flat die was used in the riveting process.

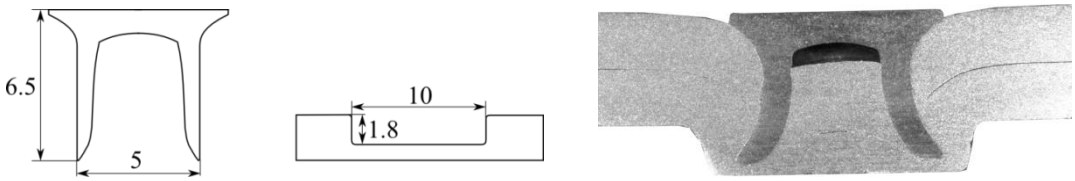

Fig. 18: Geometry and cross-section of rivet.

Single connector tests

High repeatability was obtained in the tests with SPR. To highlight the differences between FDS and SPR connections, representative curves are presented herein.

The results from the single connector tests are shown in Fig. 19. Generally, the SPR connection was stronger than the FDS connection. It should be emphasized that the nominal diameter of the screws was 4 mm while it was 5 mm for the rivets. Additionally, the legs of the rivets expand during the riveting process (see Fig. 18), resulting in an effectively larger connection diameter than for the FDS connection. Accordingly, a higher strength was expected. The observed deformation and failure modes of the SPR connections were in accordance with the observations of Porcaro et al. (2006a).

Cross test results are compared in Fig. 19 a). For tensile and mixed mode loading the ductility was highest for SPR compared to for FDS, while it was slightly lower than for FDS in shear. The largest differences in the force-displacement results were observed after the peak force.

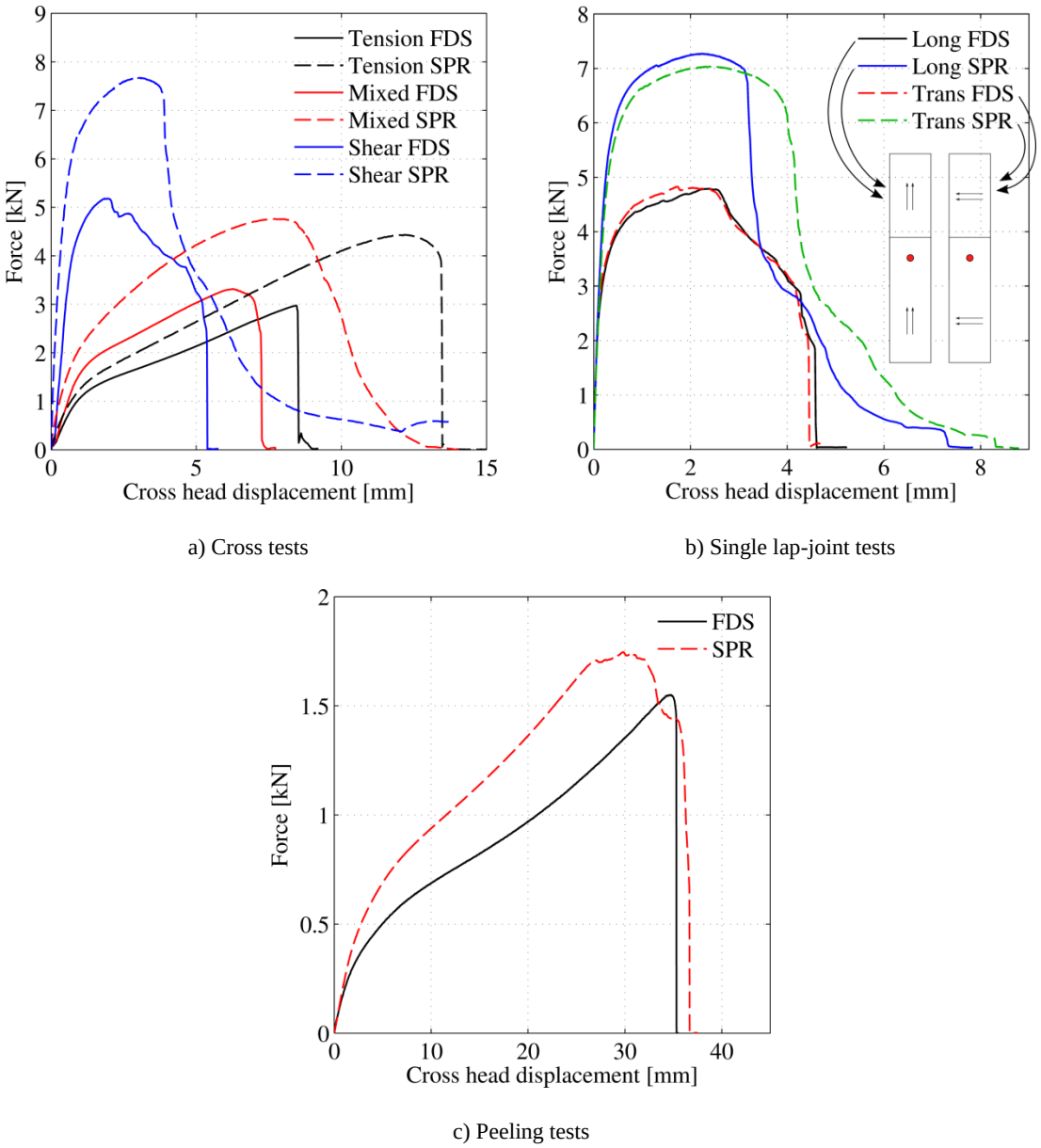

a) Cross tests

b) Single lap-joint tests

c) Peeling tests

Fig. 19: Representative force-displacement curves from single connector tests with FDS and SPR.

Under tensile loading a less abrupt failure was seen for SPR than for FDS, softening occurred before failure of the SPR connection. The rivet failed due to pull-out of the legs from the bottom sheet.

During loading in mixed mode a rotation of the rivet was observed. Failure occurred from both the top and bottom of the rivet. As the rivet rotated, the head was pulled through the top sheet when the surrounding material slowly failed, at the same time as the legs were pulled out of the bottom sheet. This occurred during the near linear decrease of force occurring after maximum force (Fig. 19 a)).

The deformation and failure of the riveted connections under shear loading were similar to what was observed under mixed mode loading. A rotation of the rivet occurred until the top sheet material failed, and the rivet legs were pulled out of the bottom sheet. After maximum force was reached, a steep force reduction was observed before the force flattened out to a plateau close to zero. In Fig. 19 b) the single lap-joint test results are compared. While no effect of the material orientation was observed for FDS, there is clearly an effect on the ductility of the SPR connection. Highest ductility was observed when the connection was loaded in the transversal material direction. A small effect was also observed on the maximum force, as slightly higher force was achieved when the connection was loaded in the longitudinal material direction.

As was the case for the FDS connection, the behaviour of the SPR connection in the single lap-joint test was similar to the behaviour in the shear cross test. The rivet rotated until the head was pulled through the top sheet, and the legs were pulled out of the bottom sheet.

The difference in strength between SPR and FDS was significantly lower in the peeling test compared to the other single connector tests (see Fig. 19 c)). This indicates that the resistance to peeling loading is relatively high for FDS connections, compared to SPR connections.

The deformation of the SPR peeling specimen was similar to the deformation observed for the FDS specimens. However, since the stiffest side of an SPR connection is the bottom side, the top sheet was bent more than the bottom sheet (opposite than for the FDS connection). Failure occurred when the head was pulled through the top sheet.

From the single connector tests it is evident that the macroscopic behaviour of FDS connections is similar to that of SPR connections under tensile, combined tensile and shear and shear loading, as well as in single lap-joint and peeling tests. The force level was higher for the SPR connections, but similar trends with respect to ductility, maximum force and shape of force-displacement curves were observed for both connections. However, the deformation and failure modes of the two connections were different.

Component tests

The dynamic force-displacement and mean force-displacement responses for SPR and FDS connections are compared in Fig. 20 a) and b). As seen, the trends are similar in terms of shape and

force levels up to approximately 60 mm displacement, after which more scatter was evident. The riveted components sustained a slightly higher force level throughout the tests, apart from the initial peak. Consequently, more energy was absorbed by the riveted components.

The increased energy absorption may be explained by the effective diameter of the SPR connection. Due to the die shape of the bottom sheet the effective diameter of the SPR connection was significantly larger than of the FDS connection. Thus, the rivet connection better prevented sheet separation during buckling (which was observed when examining the crushed specimens), leading to increased plastic deformations in the lobes of the flanges and therefore increased energy absorption.

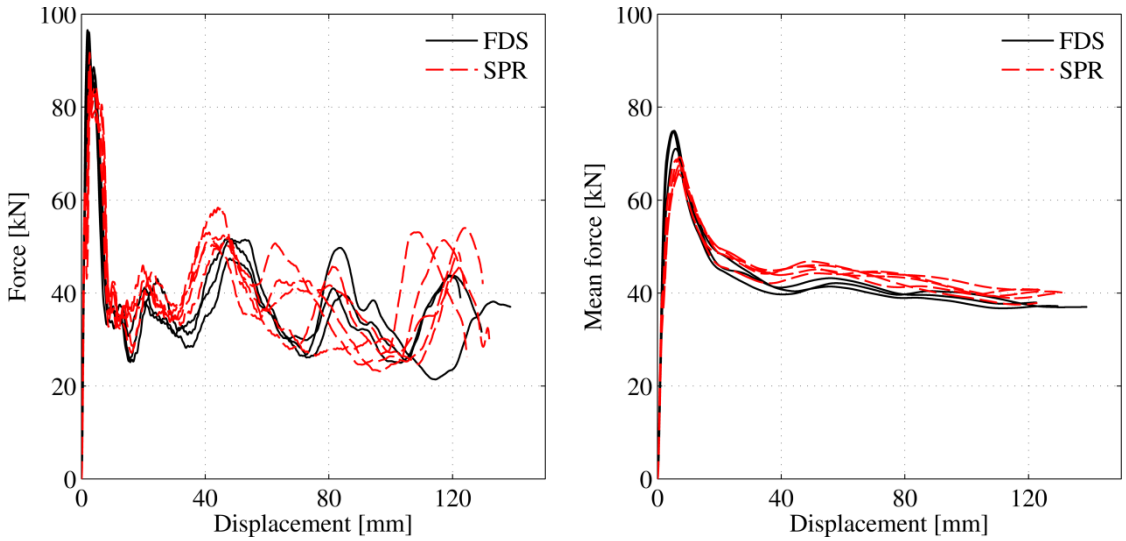

a) Force-displacement curves.

b) Mean force-displacement curves.

Fig. 20: Force-displacement (a) and mean force-displacement (b) curves from dynamic axial crushing tests with FDS and SPR connections.

The same observations were made for the quasi-static component tests. For this reason the force-displacement curves are not plotted herein. Each specimen was closely investigated after the tests. Similar differences in the buckling pattern between the dynamic and quasi-static tests were observed for SPR as was observed for FDS.

The deformation and fracture of the SPR connections in the component tests were investigated and compared to the observations for the FDS connections. In general, failure of the FDS connection was more often observed than failure of the SPR connection, and the physical deformation and failure modes of the two connection types were different.

Conclusions

The following main conclusions can be drawn from the single connector tests of flow-drill screw connections:

- The strength of the connections increased with the amount of shear loading, while the ductility decreased.
- Under tensile and combined tensile and shear loadings failure occurred by thread stripping from the bottom sheet material, while in the shear tests failure occurred by through thickness shear fracture of the bottom sheet material.
- No effect of anisotropy of the sheet material was observed on the behaviour of the connections.

For the component tests with flow-drill screws the following was found:

- Four deformation and failure modes of the screw connections were observed: screw rotation, screw pull-out, screw push-out and screw fracture. Screw push-out and screw fracture was not observed in the single connector tests.

The comparison with self-piercing rivet connections revealed the following main conclusion:

- Similar trends with respect to ductility, maximum force and shape of force-displacement curves were observed for the two connections. Largest differences were observed under shear dominated loadings. However, the underlying physical deformation and failure phenomena were different.

Acknowledgements

Acknowledgments are made to Honda R&D Americas, Inc. and Department of Structural Engineering at Norwegian University of Science and Technology (NTNU) for financial support.

References

Arcan, L., Arcan, M., Daniel, I.M., 1987. SEM fractography of pure and mixed mode interlaminar fracture in graphite/epoxy composites. ASTM Special Technical Publication 948, 41-67.

Briskham, P., Blundell, N., Han, L., Hewitt, R., Young, K., Boomer, D., 2006. Comparison of self-pierce riveting, resistance spot welding and spot friction joining for aluminium automotive sheet. SAE SP 2034, 105.

CEN, 2007. Eurocode 9: Design of aluminium structures - Part 1-1: General structural rules.

Di Lorenzo, G., Landolfo, R., 2004. Shear experimental response of new connecting systems for cold-formed structures. Journal of constructional steel research 60, 561-579.

EJOT, www.ejot.de.

Hanssen, A., Auestad, T., Tryland, T., Langseth, M., 2003. The kicking machine: A device for impact testing of structural components. International Journal of Crashworthiness 8, 385-392.

Head, G.D., Master, W.C.L., Bredesky, L.P., Winter, D.C., 1984. For forming a hole and a brushing in a metal workpiece. Google Patents.

Lademo, O.-G., Engler, O., Keller, S., Berstad, T., Pedersen, K., Hopperstad, O., 2009. Identification and validation of constitutive model and fracture criterion for AlMgSi alloy with application to sheet forming. Materials & Design 30, 3005-3019.

Langrand, B., Combescure, A., 2004. Non-linear and failure behaviour of spotwelds: a "global" finite element and experiments in pure and mixed modes I/II. International Journal of Solids and Structures 41, 6631-6646.

Langrand, B., Markiewicz, E., 2010. Strain-rate dependence in spot welds: Non-linear behaviour and failure in pure and combined modes I/II. International Journal of Impact Engineering 37, 792-805.

Langrand, B., Patronelli, L., Deletombe, E., Markiewicz, E., Drazetic, P., 2002. Full scale experimental characterisation for riveted joint design. Aerospace science and technology 6, 333-342.

Lee, Y.-L., Wehner, T., Lu, M.-W., Morrissett, T., Pakalnins, E., 1998. Ultimate strength of resistance spot welds subjected to combined tension and shear. Journal of Testing and Evaluation 26, 213-219.

Lennon, R., Pedreschi, R., Sinha, B., 1999. Comparative study of some mechanical connections in cold formed steel. Construction and Building Materials 13, 109-116.

Miller, S.F., Shih, A.J., 2006. Friction Drilling: A Chipless Hole-Making Process, ASME 2006 International Manufacturing Science and Engineering Conference. American Society of Mechanical Engineers, pp. 911-918.

Moore, M., Bate, P., 2002. Microstructural inhomogeneity and biaxial stretching limits in aluminium alloy AA6016. Journal of materials processing technology 125, 258-266.

Pedreschi, R., Sinha, B., 1996. The potential of press-joining in cold-formed steel structures. Construction and Building Materials 10, 243-250.

Porcaro, R., Hanssen, A., Aalberg, A., Langseth, M., 2004. Joining of aluminium using self-piercing riveting: testing, modelling and analysis. International Journal of Crashworthiness 9, 141-154.

Porcaro, R., Hanssen, A., Langseth, M., Aalberg, A., 2006a. The behaviour of a self-piercing riveted connection under quasi-static loading conditions. International journal of solids and structures 43, 5110-5131.

Porcaro, R., Hanssen, A., Langseth, M., Aalberg, A., 2006b. An experimental investigation on the behaviour of self-piercing riveted connections in aluminium alloy AA6060. International Journal of Crashworthiness 11, 397-417.

Porcaro, R., Langseth, M., Hanssen, A., Zhao, H., Weyer, S., Hooputra, H., 2008. Crashworthiness of self-piercing riveted connections. International Journal of Impact Engineering 35, 1251-1266.

Sun, X., Khaleel, M.A., 2005. Performance optimization of self-piercing rivets through analytical rivet strength estimation. Journal of manufacturing processes 7, 83-93.

Sun, X., Khaleel, M.A., 2007. Dynamic strength evaluations for self-piercing rivets and resistance spot welds joining similar and dissimilar metals. International journal of impact engineering 34, 1668-1682.

Szlosarek, R., Karall, T., Enzinger, N., Hahne, C., Meyer, N., 2013. Mechanical Testing of Flow Drill Screw Joints Between Fibre-Reinforced Plastics and Metals. Materials Testing 55, 737-742.

Wung, P., 2001. A force-based failure criterion for spot weld design. Experimental Mechanics 41, 107-113.

Wung, P., Walsh, T., Ourchane, A., Stewart, W., Jie, M., 2001. Failure of spot welds under in-plane static loading. Experimental Mechanics 41, 100-106.